PHYSICAL REVIEW D **76,** 094018 (2007)

$\gamma^* p$ cross section from the dipole model in momentum space

J. T. de Santana Amaral* and M. B. Gay Ducati†

Instituto de Física, Universidade Federal do Rio Grande do Sul, Caixa Postal 15051, 91501-970 - Porto Alegre, RS, Brazil

M. A. Betemps‡

Instituto de Física, Universidade Federal do Rio Grande do Sul, Caixa Postal 15051, 91501-970 - Porto Alegre, RS, Brazil and Conjunto Agrotécnico Visconde da Graça, Universidade Federal de Pelotas, Caixa Postal 460, 96060-290 - Pelotas, RS, Brazil

G. Soyez§

LPTHE, Université Pierre et Marie Curie (Paris 6), Université Diderot (Paris 7), Tour 24-25, 5e Etage, Boîte 126, 4 place Jussieu, F-75252 Paris Cedex 05, France

(Received 12 December 2006; published 16 November 2007)

We reproduce the deep inelastic scattering measurements of the proton structure function at high energy from the dipole model in momentum space. To model the dipole-proton forward scattering amplitude, we use the knowledge of asymptotic solutions of the Balitsky-Kovchegov equation, describing high-energy QCD in the presence of saturation effects. The comparison of our results with previous analysis in coordinate space and possible extensions of our approach are discussed.

DOI: 10.1103/PhysRevD.76.094018 PACS numbers: 12.38.−t, 24.85.+p

I. INTRODUCTION

One of the most intriguing problems in quantum chromodynamics (QCD) is the growth of the cross sections for hadronic interactions with energy. As is well known, the increase of energy causes a fast growth of the gluon density and consequently of the cross sections. At very high energies, this growth should not continue indefinitely and at some point one has to deal with gluon recombination and multiple scattering in order to restore unitarity. This interaction between overlapping partons is called saturation and has deserved active studies over the past 30 years [1–6].

More generally, the large amount of work devoted to the description and understanding of perturbative QCD in the high-energy limit covers the description of saturation on the theoretical side as well as its applications to phenomenology. The theoretical contribution comes mainly from the development of nonlinear QCD equations describing the evolution of scattering amplitudes towards this limit, together with the search of the solutions to those equations. The simplest of such equations is the Balitsky-Kovchegov (BK) equation [7,8], which corresponds to the Balitsky-Fadin-Kuraev-Lipatov (BFKL) [9] linear evolution equation with the addition of a nonlinear term responsible for the saturation of the growth of gluon density. It has been shown [10] that the BK equation is in the equivalence class of the Fisher-Kolmogorov-Petrovsky-Piscounov (FKPP) nonlinear partial differential equation [11], which admits traveling-wave solutions, translating, in terms of QCD variables, into *geometric scaling*, as will be explained below.

From the phenomenological side, the geometric scaling has been observed at the DESY ep collider HERA, in the measurements on inclusive $\gamma^* p$ scattering [12]. This phenomenological feature of high-energy deep inelastic scattering (DIS) is expressed as a scaling property of the virtual photon-proton cross section

$$\sigma^{\gamma^* p}(Q^2, Y) = \sigma^{\gamma^* p}\left(\frac{Q^2}{Q_s^2(Y)}\right); \tag{1}$$

that is, the cross section depends on the scaling variable $\tau = Q^2/Q_s^2(Y)$ instead of Q^2 and $Q_s^2(Y)$ separately. Here Q^2 is the virtuality of the photon, $Y = \log(1/x)$ is the total rapidity, x is the Bjorken x, related to the center-of-mass energy through $s = Q^2/x$, and $Q_s(Y)$ is an increasing function of Y called the *saturation scale*. The geometric scaling is actually equivalent to the formation of traveling-wave solutions for the BK equation. This is thus a remarkable consequence of saturation, which extends arbitrarily far beyond the fully saturated domain, i.e., in the dilute regime where saturation effects may seem negligible.

In this paper, the dipole model [13] is used to relate the $\gamma^* p$ cross section to the dipole-proton forward scattering. This approach has already been proven successful, e.g., in [14–16]. Our approach here is to parametrize the dipole-proton amplitude in momentum space, where the traveling waves have been originally derived. In this way, our parametrization will have all constraints imposed by high-energy QCD, including the geometric-scaling property. We shall discuss the advantages of our method and compare it with previous results in the literature later on.

The plan of this paper is as follows. In Sec. II, we relate the $\gamma^* p$ cross section to the dipole-proton scattering am-

*thiago.amaral@ufrgs.br
†beatriz.gay@ufrgs.br
‡marcos.betemps@ufpel.edu.br
§On leave from: University of Liège, Belgium. g.soyez@ulg.ac.be

plitude within the dipole framework. We then discuss, in Sec. III how one can describe the dipole scattering amplitude from the properties of the BK equation. In Sec. IV A we gather all information to build the complete model for the proton structure function. The fitting procedure used to compare our model with the experimental measurements is explained in Sec. IV B and the results of the fit are presented in Sec. IV C. The link with previous approaches in the literature and possible situations in which our work can find interesting applications are discussed in Sec. V.

II. THE DIPOLE MODEL

We consider the collision between a virtual photon and a proton at high energy. In a frame where the photon travels fast, one can consider that it fluctuates into a $q\bar{q}$ dipole. The lifetime of this dipole being much longer than the time of interaction with the proton, one can write the cross section as a product of the wave function for a photon to go into a dipole times the dipole-proton cross section, as shown in Fig. 1. It leads to the well-known formula

$$\sigma_{T,L}^{\gamma^* p}(Q^2, Y) = \int d^2r \int_0^1 dz |\Psi_{T,L}(r, z; Q^2)|^2 \sigma_{\mathrm{dip}}^{\gamma^* p}(r, Y), \tag{2}$$

where $\sigma_{\mathrm{dip}}^{\gamma^* p}(r, Y)$ is the dipole-proton cross section. The transverse and longitudinal photon wave functions in this expression are computable in perturbative QED. They are given by

$$|\Psi_T(r, z; Q^2)|^2 = \frac{N_c \alpha_{em}}{2\pi^2} \sum_q e_q^2 \{[z^2 + (1-z)^2] \bar{Q}_q^2 K_1^2(\bar{Q}_q r) + m_q^2 K_0^2(\bar{Q}_q r)\}, \tag{3}$$

$$|\Psi_L(r, z; Q^2)|^2 = \frac{N_c \alpha_{em}}{2\pi^2} \sum_q e_q^2 \{4Q^2 z^2 (1-z)^2 K_0^2(\bar{Q}_q r)\}, \tag{4}$$

where N_c is the number of colors, $\bar{Q}_q^2 = z(1-z)Q^2 + m_q^2$, m_q the mass of the quark of flavor q, and $K_{0,1}$ are the McDonald functions of rank 0 and 1, respectively. This expression extends the Kovchegov formula [Eqs. (4), (5a), and (5b) in the second reference of [8]] by including the mass of the quarks.

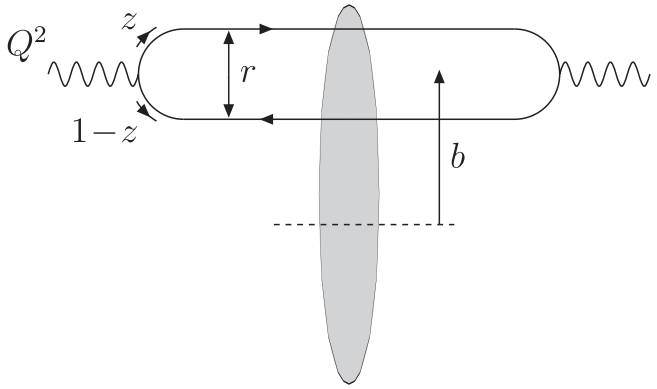

FIG. 1. Picture representing the dipole model.

If one treats the proton as a homogeneous disk of radius R_p, the dipole-proton cross section in Eq. (2) is usually taken to be proportional to the dipole-proton forward scattering amplitude $T(r, Y)$ through the relation

$$\sigma_{\mathrm{dip}}^{\gamma^* p}(r, Y) = 2\pi R_p^2 T(r, Y).$$

The proton structure function F_2 can be obtained from the $\gamma^* p$ cross section through the relation

$$F_2(x, Q^2) = \frac{Q^2}{4\pi^2 \alpha_{em}} [\sigma_T^{\gamma^* p}(x, Q^2) + \sigma_L^{\gamma^* p}(x, Q^2)]. \tag{5}$$

As we shall see in the next section, the BK equation describes the high-energy evolution of the dipole-proton scattering amplitude T. However, the asymptotic behavior of its solutions is naturally expressed in momentum space. Hence, we want to express the $\gamma^* p$ cross section in terms of $T(k, Y)$, the Fourier transform of $T(r, Y)$:

$$T(k, Y) = \frac{1}{2\pi} \int \frac{d^2r}{r^2} e^{i\mathbf{k}\cdot\mathbf{r}} T(r, Y) = \int_0^\infty \frac{dr}{r} J_0(kr) T(r, Y). \tag{6}$$

After a bit of algebra, we obtain the following expression relating the proton structure function to $T(k, Y)$:

$$F_2(x, Q^2) = \frac{Q^2 R_p^2 N_c}{4\pi^2} \int_0^\infty \frac{dk}{k} \int_0^1 dz |\tilde{\Psi}(k^2, z; Q^2)|^2 T(k, Y), \tag{7}$$

where the wave function is now expressed in momentum space

$$\begin{aligned} |\tilde{\Psi}(k^2, z; Q^2)|^2 = \sum_q \left(\frac{4\bar{Q}_q^2}{k^2 + 4\bar{Q}_q^2}\right)^2 e_q^2 \Bigg\{ & [z^2 + (1-z)^2] \\ & \times \left[\frac{4(k^2 + \bar{Q}_q^2)}{\sqrt{k^2(k^2 + 4\bar{Q}_q^2)}} \operatorname{arcsinh}\left(\frac{k}{2\bar{Q}_q}\right) + \frac{k^2 - 2\bar{Q}_q^2}{2\bar{Q}_q^2} \right] + \frac{4Q^2 z^2 (1-z)^2 + m_q^2}{\bar{Q}_q^2} \\ & \times \left[\frac{k^2 + \bar{Q}_q^2}{\bar{Q}_q^2} - \frac{4\bar{Q}_q^4 + 2\bar{Q}_q^2 k^2 + k^4}{\bar{Q}_q^2 \sqrt{k^2(k^2 + 4\bar{Q}_q^2)}} \right. \\ & \left. \times \operatorname{arcsinh}\left(\frac{k}{2\bar{Q}_q}\right) \right] \Bigg\}. \end{aligned} \tag{8}$$

Having described the DIS structure function through (7), the approach used to describe the scattering amplitude $T(k, Y)$, the forward scattering amplitude in momentum space, will be presented and discussed in the next section.

III. SCATTERING AMPLITUDES IN HIGH-ENERGY QCD

Let us now consider a fast-moving colorless $q\bar{q}$ dipole of transverse size $r = |\mathbf{x} - \mathbf{y}|$, where $\mathbf{x}$ and $\mathbf{y}$ are the coordinates of the quark and antiquark, respectively, interacting with a given dense target. In the large-N_c approximation and in the mean-field approximation, the high-energy behavior of the dipole forward scattering amplitude $T(\mathbf{x}, \mathbf{y}; Y)$ follows the BK equation [7,8]. In coordinate space this equation reads

$$\partial_Y T(\mathbf{x}, \mathbf{y}; Y) = \frac{\bar{\alpha}}{2\pi} \int d^2\mathbf{z} \frac{(\mathbf{x} - \mathbf{y})^2}{(\mathbf{x} - \mathbf{z})^2 (\mathbf{z} - \mathbf{y})^2} [T(\mathbf{x}, \mathbf{z}; Y) + T(\mathbf{z}, \mathbf{y}; Y) - T(\mathbf{x}, \mathbf{y}; Y) - T(\mathbf{x}, \mathbf{z}; Y) T(\mathbf{z}, \mathbf{y}; Y)], \quad (9)$$

where $\bar{\alpha} = \alpha_s N_c/\pi$, α_s is the strong coupling constant, considered fixed. If one neglects the dependence on the impact parameter $\mathbf{b} = (\mathbf{x} + \mathbf{y})/2$ and integrates out the remaining angular dependence of $\mathbf{r}$, (9) becomes an equation for $T(r, Y)$. The latter can be expressed in momentum space using (6).

One finds that $T(k, Y)$ obeys the BK equation in momentum space

$$\partial_Y T = \bar{\alpha} \chi(-\partial_L) T - \bar{\alpha} T^2, \quad (10)$$

where

$$\chi(\gamma) = 2\psi(1) - \psi(\gamma) - \psi(1 - \gamma) \quad (11)$$

is the characteristic function of the BFKL kernel [9] and we used $L = \log(k^2/k_0^2)$ with k_0 some fixed soft scale.

In our approach, we do not want to use directly numerical solutions of (10) as the input for the dipole scattering amplitude but rather use our knowledge of the properties of its solutions to build an analytical expression for $T(k, Y)$. As we shall explain in more detail in the next section, this allows, for example, to take into account next-to-leading-order (NLO) corrections to the BFKL kernel, which provides a much better description of the data.

It has been shown [10] that, after the change of variables

$$t = \bar{\alpha} Y, \qquad x \sim \log(k^2/k_0^2), \qquad u(x, t) \propto T(k, Y), \quad (12)$$

the BK equation reduces to the FKPP equation [11] for u when its kernel (11) is approximated in the saddle point approximation, i.e., to second order in the derivative ∂_L, the so-called diffusive approximation. The FKPP equation is a well-known equation in nonequilibrium statistical physics, whose dynamics is used to describe many reaction-diffusion systems in the mean-field approximation:

$$\partial_t u(x, t) = \partial_x^2 u(x, t) + u(x, t) - u^2(x, t), \quad (13)$$

where t and x are, respectively, the time and space variables.

This equation has been extensively studied for more than 60 years and, in particular, it is known to admit traveling waves as asymptotic solutions. This means that the solution $u(x, t)$ to Eq. (13) takes the form $u(x - v_c t)$ of a front traveling to large values of x at a speed v_c without deformation.

This property of the FKPP equation is actually true if one considers the BK equation (10) with the full BFKL kernel [10]. At asymptotic rapidities, the amplitude $T(k, Y)$, instead of depending separately on k and Y, depends only on the scaling variable $k^2/Q_s^2(Y)$, where we have introduced the *saturation scale* $Q_s^2(Y) = k_0^2 \exp(v_c Y)$, measuring the position of the wave front [more precisely, it is $L_s(Y) = \log(Q_s^2/k_0^2) = v_c Y$ which measures its position].

A more detailed calculation allows also for the extraction of two additional subleading corrections, resulting in the following expression for the tail of the scattering amplitude

$$T(k, Y) \overset{k \gg Q_s}{\approx} \left(\frac{k^2}{Q_s^2(Y)}\right)^{-\gamma_c} \log\left(\frac{k^2}{Q_s^2(Y)}\right) \times \exp\left[-\frac{\log^2(k^2/Q_s^2(Y))}{2\bar{\alpha}\chi''(\gamma_c) Y}\right], \quad (14)$$

where χ'' denotes the second derivative of the BFKL kernel (11) with respect to γ and the saturation scale

$$Q_s^2(Y) = k_0^2 \exp\left(v_c Y - \frac{3}{2\gamma_c} \log(Y) - \frac{3}{\gamma_c^2} \sqrt{\frac{2\pi}{\bar{\alpha}\chi''(\gamma_c)}} \frac{1}{\sqrt{Y}}\right). \quad (15)$$

The critical parameters γ_c and v_c are obtained from the knowledge of the BFKL kernel alone and correspond to the selection of the slowest possible wave:

$$v_c = \min_\gamma \bar{\alpha} \frac{\chi(\gamma)}{\gamma} = \bar{\alpha} \frac{\chi(\gamma_c)}{\gamma_c} = \bar{\alpha} \chi'(\gamma_c). \quad (16)$$

For the leading-order BFKL kernel (11), one finds $\gamma_c = 0.6275\ldots$, and $v_c = 4.88\bar{\alpha}$.

Physically, the property of geometric scaling has deep consequences. It expresses the fact that when one moves along the saturation line, the behavior of the scattering amplitudes remains unchanged. In addition, saturation introduces naturally the scale Q_s which provides an infrared cutoff solving the infrared instability problem of the BFKL equation. The subleading corrections in (14) also have a very important role. The last term introduces an explicit dependence on the rapidity Y and hence violates geometric scaling. However, this term can be neglected when

$$\frac{\log^2(k^2/Q_s^2(Y))}{2\bar{\alpha}\chi''(\gamma_c) Y} < 1.$$

This means that geometric scaling is obtained for

$$\log(k^2/Q_s^2(Y)) \lesssim \sqrt{2\chi''(\gamma_c)\bar{\alpha}Y},$$

i.e., in a window which extends $\sqrt{Y}$ above the saturation scale. It is a remarkable property that, at high energy, the consequences of saturation are observed arbitrarily far in the tail, where $T(k, Y)$ is much smaller than 1.

IV. DESCRIPTION OF THE $\gamma^* p$ DATA

The method that will be used to describe the experimental measurements of the proton structure function can be split in three steps. We shall first build a QCD-based model for the scattering amplitude, which can directly be used in (7) to obtain F_2. Then the details concerning the remaining ingredients needed to obtain F_2 are given and we specify the data set. We finally present the results.

A. Dipole scattering amplitude

Expression (14) only gives a description of the tail of the wave front $T(k, Y) \ll 1$ ($k \gg Q_s$). In order to complete the description, we also need expressions for T around the saturation scale and at saturation. In the infrared domain, one can show, for example, by computing the Fourier transform (6) of a Heaviside function $T(r) = \Theta(rQ_s - 1)$, that the amplitude behaves like

$$T\left(\frac{k}{Q_s(Y)}, Y\right) \overset{k \ll Q_s}{=} c - \log\left(\frac{k}{Q_s(Y)}\right), \tag{17}$$

where c is an unfixed constant.

Those expressions [Eqs. (14) and (17)] describe fully the asymptotic behavior of the amplitude. In addition, they provide universal results, i.e., they are independent of the initial condition and (14) depends only on the BFKL kernel through (16). This is a powerful result as it means that corrections like NLO BFKL contributions will lead to the same analytic form with only modified parameters.

We are thus left with the matching around the saturation scale. Analytic expressions for T between the dense and dilute regimes are poorly known from the BK equation, and therefore there is need of a way to interpolate between those two regimes. A suitable way to do that is to use (14) for $k > Q_s$ and (17) for $k < Q_s$ and match the constant c to obtain a continuous distribution. However, this definition by parts would certainly introduce oscillations in the coordinate space $T(r, Y)$ which may even lead to negative amplitudes. Thus, the best way to obtain the description of the transition to the saturation region is to perform a smooth analytic interpolation between both asymptotic behaviors.

In order to obtain an interpolation model which describes the transition from the dilute regime to the saturation one, the idea is to build the latter domain from the former. We shall first build an expression which saturates to a constant without including the logarithmic factors and then reinsert those logarithmic enhancements. Our starting point is to construct an expression which is monotonically decreasing with L and which reproduces (up to the logarithmic factor), the amplitude for geometric scaling (14)

$$T_{\text{dil}} = \exp\left[-\gamma_c \log\left(\frac{k^2}{Q_s^2(Y)}\right) - \frac{L_{\text{red}}^2 - \log^2(2)}{2\bar{\alpha}\chi''(\gamma_c)Y}\right], \tag{18}$$

with

$$L_{\text{red}} = \log\left[1 + \frac{k^2}{Q_s^2(Y)}\right] \quad \text{and} \quad Q_s^2(Y) = k_0^2 e^{v_c Y}. \tag{19}$$

This result is unitarized by an eikonal,[1] i.e., $T_{\text{unit}} = 1 - \exp(-T_{\text{dil}})$, and both logarithmic behaviors in the infrared and in the ultraviolet must be reinserted. The following function gives good results:

$$T(k, Y) = \left[\log\left(\frac{k}{Q_s} + \frac{Q_s}{k}\right) + 1\right](1 - e^{-T_{\text{dil}}}). \tag{20}$$

Equations (18)–(20) determine our model for the scattering amplitude. They provide a valid and simple interpolation between the QCD constraints (14) and (17) directly coming from the BK equation. As a consequence, our parametrization encompasses the constraints imposed by high-energy QCD with saturation effects. They will be considered in the next section in order to describe the structure function F_2 given by (7).

B. Data set

We fit all the last HERA measurements of the proton structure function from H1 Collaboration [17], ZEUS Collaboration [18], with our analysis being restricted to the following kinematic range:

$$x \leq 0.01, \tag{21}$$

$$0.045 \leq Q^2 \leq 150 \text{ GeV}^2. \tag{22}$$

The first limit comes from the fact that our approach is meant to describe the high-energy amplitudes, i.e., the small x behavior; the second cut prevents one from reaching too high values of Q^2 for which Dokshitzer-Gribov-Lipatov-Altarelli-Parisi (DGLAP) corrections need to be included properly. This gives a total of 279 data points. In addition, we have allowed for a 5% renormalization uncertainty on the H1 data.

Concerning the parameters, we have kept $\gamma_c = 0.6275$ and $\bar{\alpha} = 0.2$ fixed although a particular choice for α_s only

[1]The precise expression used to perform that unitarization to a constant is a purely mathematical trick rather than a physically motivated choice. We have tested some other choices, e.g., $T_{\text{dil}}/(1 + T_{\text{dil}})$, and found similar results. We finally opted for the eikonal extrapolation because of its simplicity.

TABLE I. Results from the fit to the F_2 data, where values of the parameters with their respective errors are indicated, together with the χ^2 per data point (in the table, nop means "number of points").

Masses	k_0^2 (10^{-3} GeV^2)	υ_c	χ_c''	R_p (GeV^{-1})	χ^2/nop
$m_q = 50$ MeV, $m_c = 50$ MeV	3.782 ± 0.293	0.213 ± 0.004	4.691 ± 0.221	2.770 ± 0.045	0.960
$m_q = 50$ MeV, $m_c = 1.3$ GeV	7.155 ± 0.624	0.193 ± 0.003	2.196 ± 0.161	3.215 ± 0.065	0.988
$m_q = 140$ MeV, $m_c = 1.3$ GeV	3.917 ± 0.577	0.161 ± 0.005	2.960 ± 0.279	4.142 ± 0.167	1.071

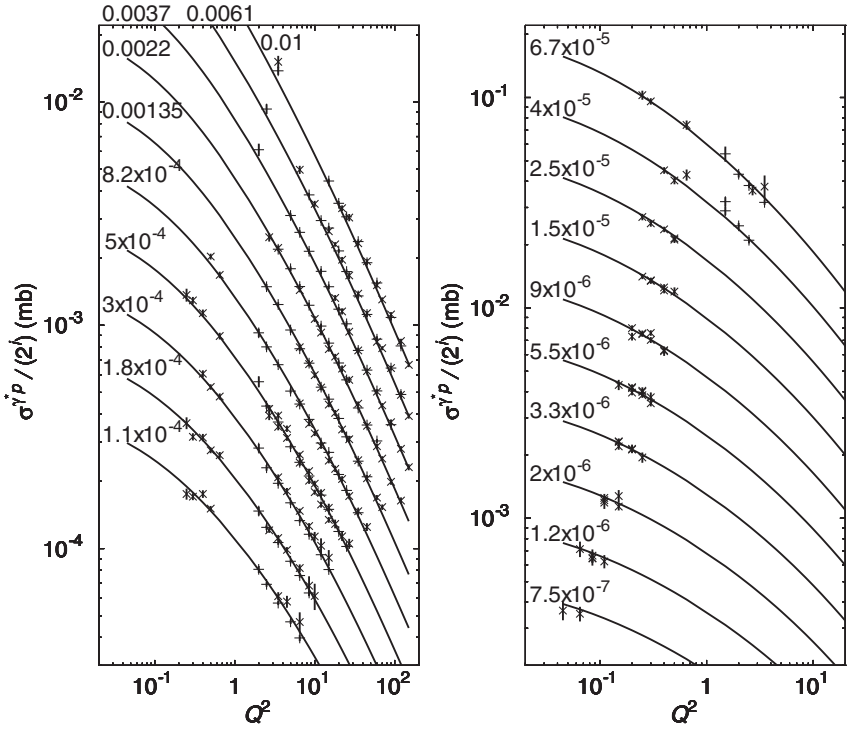

FIG. 2. Results for the fit to the virtual photon-proton cross section, where data points and the fit are shown as function of Q^2 for different values of x, indicated for each curve. For both plots, the successive curves have been rescaled by powers of 2 (1 to 2^{-9} from top to bottom) to ensure clarity. The plus corresponds to the ZEUS points, the cross to H1.

results in a renormalization of the other parameters. For the convolution with the photon wave function, different situations for the quarks masses were assumed: the light-quarks mass m_q has been set to 50 or 140 MeV while $m_c = m_q$ or $m_c = 1.3$ GeV were used for the charm mass. This leaves υ_c, χ_c'', k_0^2, and R_p as free parameters.

C. Results

The parameters obtained from the fit are shown together with the χ^2 per point in Table I. It is also plotted the comparison with the experimental data for F_2^p on Fig. 2 as well as the charm structure function F_2^c on Fig. 3. For both cases, the curves correspond to $m_q = 50$ MeV and $m_c = 1.3$ GeV. A good agreement with the measurements of F_2 is verified due to the small χ^2 provided by the fit. Moreover, the F_2^c predicted by the parametrization is in reasonable agreement with the experimental results, which shows the robustness of the model proposed in this work.

Within our parametrization, the saturation scale Q_s corresponds to the energy-dependent scale at which the dipole scattering amplitude[2] is $T(k = Q_s(Y), Y) = [1 + \log(2)](1 - 1/e) \approx 1.07$. For the fit corresponding to $m_q = 50$ MeV and $m_c = 1.3$ GeV, we obtain a saturation scale $Q_s = 0.206$ GeV for $x = 10^{-4}$ and $Q_s = 0.257$ GeV for $x = 10^{-5}$. Although these values may seem rather small, we have to emphasize that they correspond to large values for T. If, instead, we extract the saturation scale by requiring that $T = 1/2$ when $k = Q_s$, we get $Q_s = 0.296$ (respectively, $Q_s = 0.375$) GeV for $x = 10^{-4}$ (respectively, $x = 10^{-5}$). These last values are still a bit smaller than the saturation scales observed in previous studies ($Q_s \approx 1$ GeV for $x \approx 10^{-5}$) and, hence, tend to confirm the tendency for the saturation scale to decrease when

[2]Note that, when working in momentum space, the logarithmic behavior of the amplitude in the infrared allows it to take values larger than 1. This is not a contradiction with unitarity.

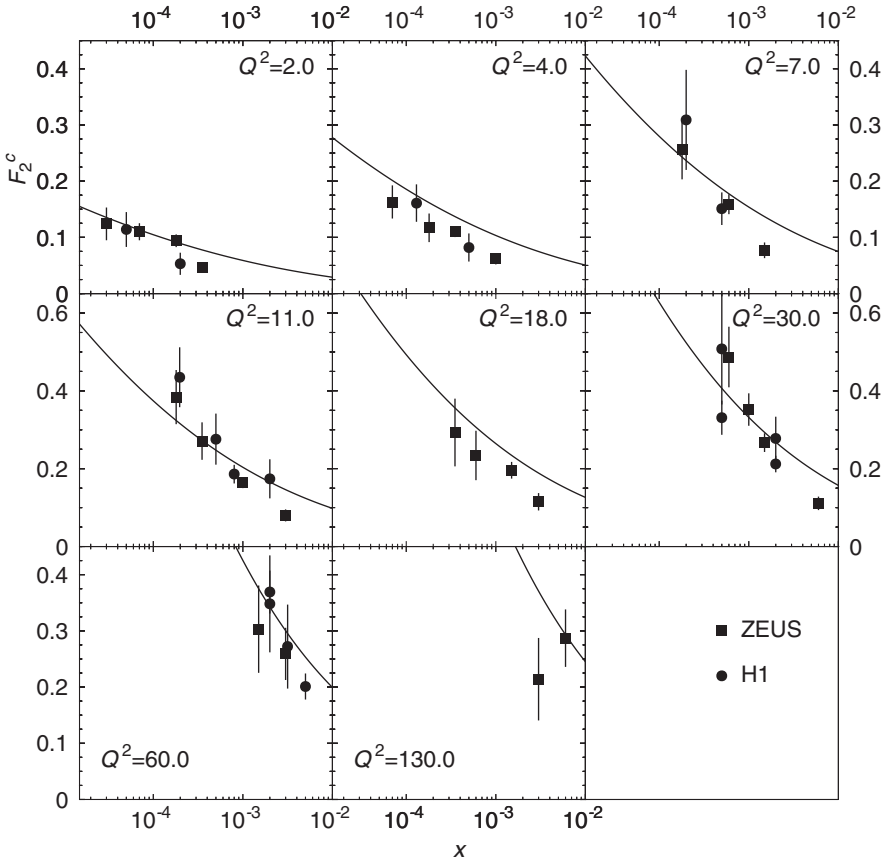

FIG. 3. Predictions for the H1 [21] and ZEUS [22] measurements of the charm structure function presented as a function of x for different values of Q^2, given in GeV^2.

heavy-quark effects are taken into account. The geometric-scaling window is thus shifted to smaller Q^2 which means that saturation corrections are less important than expected from the analysis without heavy-quark effects, especially in the vicinity of the saturation scale. Note however that for $Q^2 \ll Q_s^2$, the amplitude is fully saturated in both cases hence the prediction for F_2 remains the same.

V. CONCLUSIONS AND DISCUSSIONS

In this work we have investigated the traveling-wave solutions of the BK equation which describe the forward scattering amplitude at high energies and tested their phenomenological implications for the virtual photon-proton scattering. We have proposed an expression for the amplitude in momentum space [see Eqs. (18)–(20)] which interpolates between the behavior of the dipole-proton amplitude at saturation and the traveling-wave, ultraviolet, amplitudes predicted by perturbative QCD from the BK equation. This expression was used to compute the proton structure function F_2 (in the framework of the dipole model) and tested against the HERA data. We obtained a good fit with light quark masses $m_{u,d,s} = 50$, 140 MeV and heavy charm mass $m_c = 1.3$ GeV.

At this point, it is interesting to compare our results with those from previous approaches in the literature. In the past decade some dipole models of DIS at small x have been proposed and turned out to be successful in describing the experimental data. Among these, our comparisons were particularly focused on the pioneering Golec-Biernat-Wüsthoff (GBW) model [14], the Iancu-Itakura-Munier (IIM) model [15], and recent developments concerning the Bartels-Golec-Biernat-Kowalski (BGK) model [16,19], which consists of the GBW model improved by the incorporation of a proper gluon density evolving according to the DGLAP evolution equation. Some results from these models are shown in Table II. For each parametrization, we indicate the values used for the (light and charm) quark masses, the number of points, and the respective values of χ^2 per data point obtained from the fit.

It should be stressed that these models were developed in coordinate space and not in momentum space, as in the

TABLE II. Comparison between the results from the parametrizations in [14–16] and this work.

Parametrization	Quark masses	nop	χ^2/nop
GBW [14]	$m_q = 140$ MeV, $m_c = 1.5$ GeV	372	1.5
IIM [15]	$m_q = 140$ MeV, no charm	156	0.81
BGK [16]	$m_q = 0$ MeV, $m_c = 1.3$ GeV	288	1.06
This work	$m_q = 50$ MeV, $m_c = 1.3$ GeV	279	0.988

present work. Our choice is directly motivated by the analysis of the BK equation in momentum space leading to universal asymptotic results on which we heavily rely. Although most approaches are able to reproduce the F_2 data with a good χ^2, our model can be differentiated from the previous ones at two levels. On the one hand, our analysis is based on the BK equation to account for unitarity effects. Thus, we expect it to be more precise than the Glauber-Mueller-like approaches used in [14,16], especially, in the small-x and low-Q^2 domain under study. On the other hand, we improved the IIM model by including massive charm. Moreover, in GBW, IIM and BGK models, one finds some difficulties after performing their Fourier transform, that is, changing from the coordinate to momentum space. For IIM and GBW models such aspects were analyzed in detail in [20], and for BGK model these difficulties were pointed out in the original paper [19]. In the case of GBW model, one also obtains a Fourier transform of the dipole cross section which presents an unrealistic perturbative behavior, while in the case of IIM and BGK models it presents nonpositive values. These problems are tamed in our model, where the inverse Fourier transform (scattering amplitude in coordinate space) remains between 0 and 1. The resulting dipole cross section presents the color transparency property, i.e., $\sigma_{\rm dip} \sim r^2$ when $r \to 0$ and the saturation property, i.e., $\sigma_{\rm dip} \sim \sigma_0$ at large r.

These features associated with the good data description and small χ^2 provide that the dipole scattering amplitude proposed in this work should be a good parametrization to investigate the properties of the observables at RHIC and LHC energies, considering the dipole approach. Concerning the arbitrariness of this model, although we have observed that the results do not significantly depend upon the precise choice made for the unitarization of the amplitude, it remains interesting for further studies to see if one can get further analytic insight directly from the BK equation.

ACKNOWLEDGMENTS

This work is partially supported by CAPES (J. T. S. A.) and CNPq (M. B. G. D. and M. A. B.). G. S. is funded by the National Funds for Scientific Research (FNRS, Belgium).

[1] L. V. Gribov, E. M. Levin, and M. G. Ryskin, Phys. Rep. **100**, 1 (1983).
[2] A. H. Mueller and J. W. Qiu, Nucl. Phys. B **268**, 427 (1986).
[3] A. H. Mueller, Nucl. Phys. **B335**, 115 (1990).
[4] J. Jalilian-Marian, A. Kovner, A. Leonidov, and H. Weigert, Nucl. Phys. **B504**, 415 (1997); E. Iancu, A. Leonidov, and L. D. McLerran, Nucl. Phys. **A692**, 583 (2001); H. Weigert, Nucl. Phys. **A703**, 823 (2002).
[5] A. L. Ayala, M. B. Gay Ducati, and E. M. Levin, Nucl. Phys. **B493**, 305 (1997); **B511**, 355 (1998).
[6] Y. V. Kovchegov and A. H. Mueller, Nucl. Phys. **B529**, 451 (1998).
[7] I. Balitsky, Nucl. Phys. **B463**, 99 (1996); Phys. Rev. Lett. **81**, 2024 (1998); Phys. Lett. B **518**, 235 (2001); arXiv:hep-ph/0101042.
[8] Y. V. Kovchegov, Phys. Rev. D **60**, 034008 (1999); **61**, 074018 (2000).
[9] L. N. Lipatov, Sov. J. Nucl. Phys. **23**, 338 (1976); E. A. Kuraev, L. N. Lipatov, and V. S. Fadin, Sov. Phys. JETP **45**, 199 (1977); I. I. Balitsky and L. N. Lipatov, Sov. J. Nucl. Phys. **28**, 822 (1978).
[10] S. Munier and R. Peschanski, Phys. Rev. Lett. **91**, 232001 (2003); Phys. Rev. D **69**, 034008 (2004); **70**, 077503 (2004).
[11] R. A. Fisher, Ann. Eugenics **7**, 355 (1937); A. Kolmogorov, I. Petrovsky, and N. Piscounov, Moscow Univ. Math. Bull. A **1**, 1 (1937).
[12] A. M. Stasto, K. Golec-Biernat, and J. Kwiecinski, Phys. Rev. Lett. **86**, 596 (2001); F. Gelis, R. Peschanski, G. Soyez, and L. Schoeffel, Phys. Lett. B **647**, 376 (2007).
[13] A. H. Mueller, Nucl. Phys. **B415**, 373 (1994); A. H. Mueller and B. Patel, Nucl. Phys. **B425**, 471 (1994); A. H. Mueller, Nucl. Phys. **B437**, 107 (1995).
[14] K. Golec-Biernat and M. Wusthoff, Phys. Rev. D **59**, 014017 (1998).
[15] E. Iancu, K. Itakura, and S. Munier, Phys. Lett. B **590**, 199 (2004).
[16] K. Golec-Biernat and S. Sapeta, Phys. Rev. D **74**, 054032 (2006).
[17] C. Adloff *et al.* (H1 Collaboration), Eur. Phys. J. C **21**, 33 (2001).
[18] J. Breitweg *et al.* (ZEUS Collaboration), Phys. Lett. B **487**, 273 (2000); S. Chekanov *et al.* (ZEUS Collaboration), Eur. Phys. J. C **21**, 443 (2001).
[19] J. Bartels, K. Golec-Biernat, and H. Kowalski, Phys. Rev. D **66**, 014001 (2002).
[20] M. A. Betemps and M. B. Gay Ducati, Phys. Rev. D **70**, 116005 (2004).
[21] C. Adloff *et al.* (H1 Collaboration), Phys. Lett. B **528**, 199 (2002); A. Aktas *et al.* (H1 Collaboration), Eur. Phys. J. C **45**, 23 (2006).
[22] S. Chekanov *et al.* (ZEUS Collaboration), Phys. Rev. D **69**, 012004 (2004).